The Lorentz force and the nature of charge from a photonic toroidal vortex model

Barry R. Clarke
ORCID: https://orcid.org/0000-0003-4131-4324

Abstract
In 1865, Maxwell characterized a magnetic field line as an axis of angular momentum. It is shown why this cannot provide an *explanation* for the migration of charge and the generation of an emf in a conductor moving perpendicularly through these lines. The Lorentz force deflection is instead derived from the photonic toroidal vortex (PTV) model developed by Clarke (2025). The model defines a mass in terms of optical orbital angular momentum (OAM) with a specific beam waist, and here it is shown how motion towards a magnetic field line with a gradient creates a change in momentum perpendicular to it, resulting in an excess or deficit of action in the mass's OAM circuit. This is redistributed into motion along the OAM axis. The mean value of these redistributions, averaged over all OAM positions in the PTV rotation, results in the Lorentz force deflection. In the process, a geometrical nature of electric charge is suggested in terms of a combination of OAM and toroidal rotation senses.

Keywords*: string theory; Lorentz force; photonics; optical spin angular momentum, optical orbital angular momentum; photonic toroidal vortex; charge*

Contents

B. R. Clarke
Oxford, UK

aleteller@barryispuzzled.com

1 Introduction

Most graduates of physics are familiar with the well-known Lorentz force law

$$\vec{F} = q\vec{v} \times \vec{B} \tag{1}$$

where q is the charge passing through a magnetic field $\vec{B}$ with velocity $\vec{v}$. However, while it provides a 'rule of association' for the deflection effect, it offers no insight into the geometrical nature of charge.[1] It merely describes what is seen on a macroscopic level. It also turns out that there is a crucial inconsistency at the heart of Maxwell's derivation of the Lorentz force (as it was later known) in that a magnetic field line serves as an axis of angular momentum thus

$$\vec{B} = \nabla \times \vec{A} \tag{2}$$

where $\vec{A}$ is the vector potential or the momentum per unit charge. To see this, for a rotation with angular velocity ω around the z axis, since the velocity $\vec{v} = \vec{\omega} \times \vec{r}$ then $\nabla \times \vec{v} = 2\omega\hat{k}$. The momentum per unit charge can be written as $\vec{A} = m\vec{v}/q$ so $\vec{B} = \nabla \times \vec{A}$ becomes $\vec{B} = 2m\omega\hat{k}/q$. For a symmetrical object, the angular momentum $\vec{L} = I\vec{\omega}$ where I is the moment of inertia. Then with $\vec{\omega} = \omega\hat{k}$ we have $\vec{B} = 2m\vec{L}/qI$. That is, the vector $\vec{B}$ shares an axis of rotation with angular momentum $\vec{L}$.[2] The objection we shall raise here against the nature of $\vec{B}$ creates a need for a re-examination of what this vector represents. In this paper, the principles of a recently developed photonic toroidal vortex (PTV) model [2] will be used to obtain Eq. (1), identify the magnetic field line $\vec{B}$ as a flow of field momentum, and reframe the nature of charge in terms of rotation combinations of optical orbital angular momentum (OAM) and toroidal rotation.

Optical SAM was demonstrated by Beth in 1936 who showed that light exerts a torque on a rotating half-wave plate as its circular polarization is reversed [3].[3] Subsequent experiments managed to replicate the effect [4–7]. Optical OAM can be created in the laboratory by diverting the trajectory of optical SAM into a pseudo-cylindrical beam with a phase that is dependent on azimuthal angle.[4] Spiral wave plates [8], holograms [9–11], and cylindrical lenses [12–15] have all been used to create a helical phase structure from the diversion of linear rays. In 1992, Allen et al. predicted that in the paraxial approximation, a beam that possesses both SAM and OAM should convey a torque

$$T = P_{abs}(l + \sigma_z)/\omega \tag{3}$$

where P_{abs} is the power absorbed by a material fragment (proportional to the number of photons absorbed per second), $l\hbar$ is the OAM per photon with l a non-zero integer, $\sigma_z = \pm 1$ for left- and right-circularly polarized light, and ω is the angular velocity [14]. The transfer of OAM from a linearly polarized LG mode laser to trapped CuO particles was subsequently observed by He et al. [11],[5] and by Friese et al. using a combination of SAM and OAM [16].[6] The latter work corroborated Eq. (3) in that when SAM is introduced to a rotation frequency of a fragment created by OAM, it increases when the spin and orbital rotations reinforce, and decreases when their rotations are in opposition [16]. A more efficient experiment that allowed the whole of the beam to participate was performed by Simpson et al. who used weakly absorbing Teflon fragments 2μm in

[1] A 'rule of association' merely relates the causal variables to the effect variable with no attendant mechanism. Ampère's law and Coulomb's law are similar rules.

[2] In §2154 of his *Experimental Researches* Faraday discusses the Faraday Effect in which magnetic field lines passing through a diamagnetic rotate the plane of polarized light passing along these lines. He says "the character of the force thus impressed upon the diamagnetic is that of *rotation* […]" [1]. However, the magnetic field lines are not necessarily conveying a rotation that they possess. They could be causing the diamagnetic to induce one.

[3] Beth found that with a clockwise rotating plate, the incident rcp wave polarization changes to lcp, the wave frequency is reduced, and the plate gains angular momentum. Also, lcp turns into rcp, the wave frequency is increased, and the plate loses angular momentum.

[4] The theory developed in Ref. [2] suggests that at an atomic level the SAM trajectory *curves* around a notional tube.

[5] The absorbing particles were black superconductor ceramic powder of size $1 - 2\mu$m soaked in kerosene.

[6] The particles were CuO of size $1 - 5\mu$m soaked in kerosene.

diameter in a three-dimensional optical spanner [15].[7] In 80% of their trials, when the SAM and OAM reinforced the fragments speeded up, most of them doubling their angular velocities. The fragments became stationary when the SAM and OAM rotations were in opposition. So both optical SAM and OAM have been demonstrated to produce mechanical effects.

A photonic toroidal vortex (PTV) has been created in the laboratory that allows optical OAM to run around the surface of a toroid and occupy the whole surface [17]. Without recourse to either quantum mechanics or classical electrodynamics, a PTV theory has been developed based on the OAM of a helical string that obtains an accurate fine structure spectrum for the hydrogen atom [2]. This theory defines an internal potential to accommodate the fact that electron vortices have been found to adopt discrete OAM states in the absence of an external potential [18–20]. More recent work has extended it the hyperfine structure [21]. In the present work, we make use of the principles introduced in the internal-potential PTV theory [2] to present a visualizable *explanation* of the Lorentz force deflection and to suggest the geometrical nature of charge. The consequences of this identification for the electrical and magnetic momentum fields in PTV theory [2, 21] are discussed.

2 The inconsistency in Maxwell's derivation

The first equations for the deflection of a charge passing through magnetic field lines were given by Maxwell in March 1861 [22, Eq. (77)] in Part II of a four-part paper 'On physical lines of force'. Four years later, Maxwell changed the signs on the time derivatives of the magnetic vector potential components F, G, H from positive to negative to obtain Eqs. (4) [23]. Previously, Maxwell had introduced his displacement current which required a sign-change in the vector potential in order to derive the wave equation.[8] His equations for the components P, Q, R of the electromotive force $\vec{E}$, he gave as

$$\begin{aligned} P &= \mu\gamma\frac{dy}{dt} - \mu\beta\frac{dz}{dt} - \frac{dF}{dt} - \frac{d\Psi}{dx} \\ Q &= \mu\alpha\frac{dz}{dt} - \mu\gamma\frac{dx}{dt} - \frac{dG}{dt} - \frac{d\Psi}{dy} \\ R &= \mu\beta\frac{dx}{dt} - \mu\alpha\frac{dy}{dt} - \frac{dH}{dt} - \frac{d\Psi}{dz} \end{aligned} \tag{4}$$

where α, β, γ are Maxwell's components of the magnetic intensity $\vec{H}$, μ is the coefficient of magnetic induction, F, G, H are his components of the magnetic vector potential $\vec{A}$ (magnetic momentum per unit charge), and Ψ is the electric potential ϕ. When *A Treatise on Electricity and Magnetism* appeared in 1873, Maxwell derived Eqs. (4) by making use of Faraday's law of induction in the context of the magnetic effect of a secondary circuit on a primary [25, Art. 598], see Yaghjian (2020) for an exposition in modern notation [26].[9]

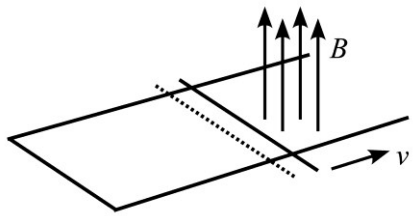

FIG. 1 Straight wire sliding at speed v on two parallel wires that form a circuit, to pass through perpendicular magnetic field lines $\vec{B}$.

[7] An optical spanner uses Laguerre-Gaussian laser modes with optical OAM to obtain a tightly focused beam that can trap particles.
[8] Maxwell's displacement current appeared in Part III of his work [24]. It was meant to represent a displacement of charge in an aether that was later shown to be superfluous. It's only use is to derive the wave equation.
[9] In 1889, Heaviside quotes "Maxwell's 'electromagnetic force'" as $\mathbf{F} = \mu_o q \mathrm{V}\mathbf{u}\mathbf{H}_o$, where he uses V to denote a vector product [27].

In his analysis, Maxwell considers a straight wire sliding perpendicularly on two parallel rails that are connected at one end to form a closed circuit, see Fig. 1. If the circuit is considered to be in a specific plane, the magnetic field lines $\vec{B}$ run normal to that plane. The local length of the wire, velocity v of the wire, and the magnetic field lines are mutually perpendicular. The aim is to evaluate the sum of the scalar products of the time-rate-of-change of the magnetic vector potential $\vec{A}$ — which Maxwell calls "electrokinetic momentum" [25, Art. 590] — and the circuit length increment in a line integral. It is essentially a sum of increments of the time-rate-of-change of action per unit charge taken around the circuit and this is Maxwell's starting point. The electromotive force is the rate of decrease of action around the circuit [25, Art. 579]. To arrive at the Lorentz force law (as it was later called), Maxwell's method relies on the representation of a magnetic field line as the axis of rotation of an angular momentum per unit charge using $\vec{B} = \nabla \times \vec{A}$ because without this relation he cannot introduce the vector $\vec{B}$ into the law [26]. However, we shall now see that although in practice there is an emf generated by a change in field lines, in theory, a rotation of momentum per unit charge around these field lines cannot account for it.[10] This suggests that these rotations do not actually exist.

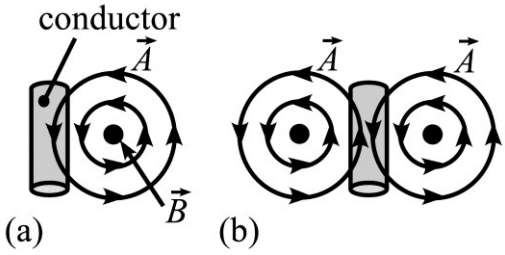

FIG. 2 a A changing magnetic field line $\vec{B}$ (running out of the page) with circulating changing vector potential $\vec{A}$ cutting an increment of conducting wire producing an emf. **b** When the $\vec{B}$ field lines are on both sides of the conducting increment there is no net emf due to opposition of the vector potential rotations.

Consider an increment of conducting wire with a field line adjacent and perpendicular to it on one side, Fig. 2a. In order to change $\vec{A}$, the momentum per unit charge, either a change in field strength is introduced along the direction of $\vec{B}$, or relative motion through space substitutes the line $\vec{B}$ with another one that takes up the same position relative to the conducting increment. The part of the change in angular momentum rotation adjacent to the wire communicates momentum to the charges generating an emf. Now let us add a parallel $\vec{B}$ field line adjacent to the wire on the opposite side, Fig. 2b. The two change-in-momentum rotations now cancel out and there is no emf. Increments of wire can be added to our conductor end-to-end to form a closed circuit with a similar field line on each side of each increment. Since all increments behave alike, there is no net emf generated.[11] Nevertheless, when in practice the field lines are changed around a conducting loop — and they must manifest both inside and outside of the closed circuit — an emf is *measured* to occur. This means that the notion of a vector potential $\vec{A}$ circulating a field line $\vec{B}$ is incapable of accounting for it.[12] So there needs to be a re-examination of the nature of a $\vec{B}$ field line emanating from a magnetic north pole or solenoid.

[10] It is irrelevant that when we invoke Stokes' law, confine ourselves to the $\vec{B}$ field lines inside the closed-circuit aperture, and suppose there to be rotations around the lines (some parts of which cancel out) that we obtain a reasonable prediction of the emf. Our concern here is with an *explanation*, and these rotations fail to provide one.

[11] If the increments form a closed loop and the field lines are equally spaced there should be more curve-contiguous lines outside the curve than inside and the charge migration would be oppositely directed to that observed.

[12] I suspect that this objection had already occurred to Heaviside. He suggested abandoning Maxwell's $\boldsymbol{E} = -\dot{\boldsymbol{A}} - \nabla\Psi$ and $curl\ \boldsymbol{A} = \mu\boldsymbol{H}$ in favour of his own construction $-curl\ \boldsymbol{E} = (4\pi g + \mu d/dt)\boldsymbol{H}$, where g is "a physically non-existent quantity" and announced that "The Ψ and $\boldsymbol{A}$ are murdered, so to speak, with a great gain in definiteness and conciseness" [28].

3 Principles of the PTV method

3.1 Definition of rest mass

A model for the structure of a single photon has been proposed in which a string follows a helical trajectory at speed $\sqrt{2}c$ and rake angle $\pi/4$ so that the linear and azimuthal speed are both c, see Fig. 3a.[13] This rotation is denoted as Sp-1 and Fig. 3a shows a helical string (HS) that is left-circularly polarized. In this model, a single photon consists of an advancing array of such tubes [29]. The notional tube in Fig. 3a is then given a helical trajectory around another notional tube at speed c to produce optical OAM denoted as Sp-2. This has a linear speed βc. The Sp-2 rotation also allows a definition of the electron and proton rest mass which is defined by

$$m_o = \frac{h}{2\pi r_{2o} c} \tag{5}$$

where r_{2o} is the rest mass tube radius when $\beta c = 0$. The electron rest mass occurs for $r_{2o} = 3.861\,592\,68 \times 10^{-13}$ m while the proton rest mass has $r'_{2o} = 2.103\,089\,104 \times 10^{-16}$ m [2, Eq. (1)].

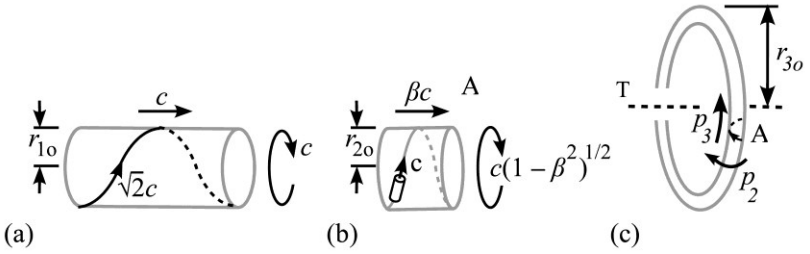

FIG. 3 a Construction of a circularly polarized ray or optical SAM (denoted as Sp-1) in which a string follows a helical trajectory around a notional tube at speed $\sqrt{2}c$. **b** Construction of optical OAM (denoted as Sp-2) in which the notional tube in Fig. 3a follows a helical trajectory at speed c around a larger notional tube, with linear speed βc. **c** A photonic toroidal vortex with the structure A in Fig. 3b rotating around a toroid with poloidal (Sp-2) momentum $p_2 = \beta c$ and toroidal (Sp-3) momentum $p_3 = c(1-\beta^2)^{1/2}$.

3.2 Momentum fields

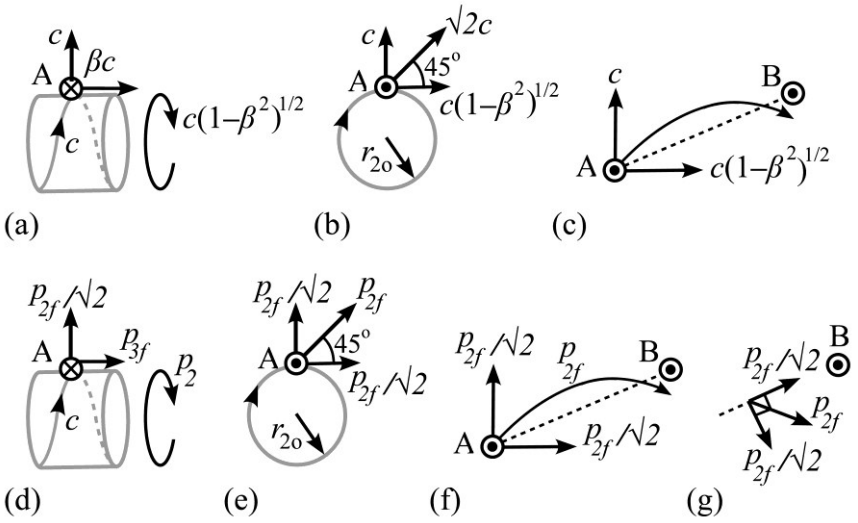

FIG. 4 Velocity and momentum field components of the Sp-2 and Sp-3 rotations. **a** The Sp-2 circuit in Fig. 3b, when situated in a toroid, emits a field throughout its trajectory, with radial speed c, Sp-3 speed βc, and Sp-2 speed $c(1-\beta^2)^{1/2}$

[13] The original model was an array of non-rotating screw threads advancing at speed c, but Ref. [2, footnote 8; 23] suggests that an array of strings each following a helical trajectory has greater possibilities. It is the latter model that is adopted here.

into the page (cross). **b** Right-end elevation of the Sp-2 in Fig. 4a in which the component at A out of the page (dot) is the Sp-3 speed βc and the resultant projection initially runs at speed $v_f = \sqrt{2}c$. **c** Trajectory of the field emission at A towards a target Sp-2 circuit at B, in which the radial direction rotates. Both the radial and Sp-2/Sp-3 speeds diminish proportionally with distance to produce a momentum p_{2f} approximately 45° to the line AB. **d** Momentum analogue of Fig. 4a. **e** Momentum analogue of Fig. 4b in which the field momentum is equally partitioned between the radial and the resultant of the Sp-2/Sp-3 directions. **f** Momentum analogue of Fig. 4c. **g** Detail of B in Fig. 4f in which the radial field component has rotated with the Sp-2 field rotation to point towards B and maintain p_{2f} at 45° to the line AB.

The model presented here assumes that both the Sp-2 and Sp-3 rotations give rise to momentum fields in the surrounding space with initial resultant speed $\sqrt{2}c$. There is a radial component to the field with speed c (Fig. 4a) that rotates with the Sp-2 momentum field (Figs 4f and 4g). An equal partitioning between the radial and the resultant of the Sp-2 and Sp-3 rotational momenta occurs at the emission point A in (Fig. 4b and 4e).[14] The radial and Sp-2 speeds diminish proportionally with distance [21, Eq. (9)] so that a 45° spiral angle to the line AB joining source and target Sp-2 circuits is maintained during field transit (Figs 4c and 4f). The Sp-2 magnetic momentum field magnitude is given by $p_{2f} = \hbar/r_{2f}$ where r_{2f} is the field radius from the Sp-2 center [2, Eq. (21)]. Since $\hbar = mr_{2o}c(1-\beta^2)^{1/2}$ [2, Eq. (6)] — $m = m_2$ is given by Ref. [2, Eq. (10)] — then the Sp-2 and Sp-3 field momenta (Ref. [2, Eqs.. (25) and (26)] vary (due to speed variation) as

$$p_{2f} = mc(1-\alpha^2)^{1/2}\,\frac{r_{2o}}{r_{2f}}, \quad p_{3f} = m\alpha c\,\frac{r_{2o}}{r_{2f}}, \quad m = \frac{m_o}{(1-\alpha^2)^{1/2}} \tag{6}$$

where r_{2o} is the radius of the Sp-2 tube and m is the relativistic mass [21, Eq. (9)]. Since $\alpha \ll 1$, given that the azimuthal speed varies inversely as r_{2f} [2, Sec. 2.7.2], the field emission begins its path at A through space at approximately angle 45° to the Sp-2 rotation-tangent in a plane *almost* perpendicular to the Sp-2 axis.[15] If we construct a straight line AB between the Sp-2 centers of the source and target (Fig. 4f), due to the rotating radial vector in Figs. 4e and 4g, the $\vec{p}_{2f}$ momentum vector is maintained at 45° to this line. This supports an earlier assumption about the 45° orientation of the proton magnetic momentum field when it strikes a distant electron Sp-2 circuit, one that is crucial to the hyperfine calculation for the hydrogen atom [21, Fig. 4b]. Although the magnetic momentum field is a Sp-2 rotation, it is the electrons' aligned Sp-3 rotations that provide the magnetic field around a current-carrying conductor.

3.3 Interaction between mass and radiation

In the PTV model, an electron is represented as a Sp-3 toroid, the Sp-3 rotation being necessary to provide the charge. Its Sp-2 rotation carries the mass. Consider a Sp-2 circuit moving with momentum $\vec{p}_e$ along its axis. This would manifest as Sp-3 rotation in an electron PTV. If a photon with momentum $\vec{p}_p$ strikes it as the rotational momentum in optical SAM or OAM, the electron momentum along its axis changes to $\vec{p}_e + \vec{p}_p \cdot \hat{p}_e$, where the latter term is a scalar product. The Sp-2 momentum rotation in the mass does not participate in mass–radiation interactions. Only the radiation momentum component along the poloidal axis (as Sp-3 rotation in a toroid) is to be considered.

3.4 Interaction between mass and field

Only *changes* in field momentum can affect a Sp-2 mass. Unlike radiation, which can only exchange momentum along the target's Sp-2 axis, a change in the magnetic momentum field must act *in the plane* of a target Sp-2 rotation as a line integral around the circuit. In the hydrogen atom hyperfine interaction [21, Eq. (36)], the proton's magnetic momentum field changes due to the proton–electron relative motion and it acts on the electron's Sp-2 rotation circuit. However, the field must have a gradient across the Sp-2 circuit otherwise there is no effect. This results in either an overload or underload of Sp-2 azimuthal action which becomes

[14] Since $|p_{3f}| \ll |p_{2f}|$ and $\beta c \ll c$, Fig. 4 is shown neglecting the participation of the Sp-3 speed and momentum in the partitioning.
[15] The Sp-3 drift speed βc is taken to be negligible here.

displaced along its axis and either adds to or subtracts from the electron's Sp-3 toroidal energy. We shall see in our derivation of the Lorentz force that it is this effect that produces the desired deflection.

3.5 Nature of the *B* field

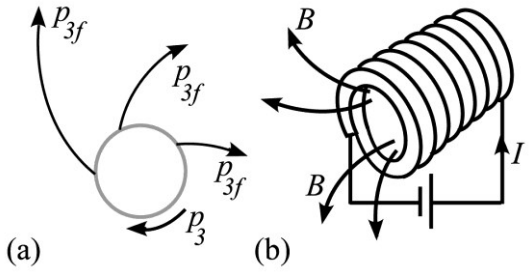

FIG. 5 a Cross section of a conducting wire with emitted Sp-3 field p_{3f}. **b** Solenoid in which the electrons are moving with surrounding B field lines.

The mapping of magnetic field lines from a magnetic north pole involves recording the strength and direction a magnetic needle takes as its position is changed in the vicinity of the pole. In 1852, Faraday confessed that the term '[B] line of force' did not include "any idea of the nature of the physical cause of the phenomena" and that "how the magnetic force is transferred through bodies or through space we know not" [30]. However, his preference was for the transmission of an influence rather than an action at a distance.

Consider the emission of magnetic field lines p_{3f} with initial speed αc ($\beta = \alpha$), Fig. 4b. Since a solenoid has electrons travelling in the opposite direction to the current I, then the B field lines p_{3f} in Fig. 5b, according to the PTV model [2] must be identical with field lines emanating perpendicular to p_{2f} in Fig. 4. When a potential difference is placed across a conducting wire, the electron Sp-3 axes align with the conductor and it is their Sp-3 electric momentum fields that rotate around the conductor. However, it does so in a spiral like the magnetic momentum field, Fig. 4f. The stronger the potential difference, the more electrons align. So, macroscopically the magnetic field in Ampère's law is an *electric* momentum field and the field lines do not adopt a closed curve (which would be a purely azimuthal field) but a spiral.

4 The Lorentz deflection

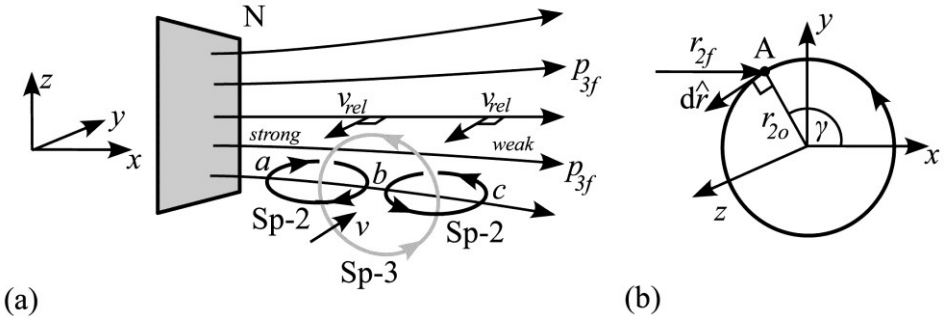

FIG. 6 a Face of a magnetic north pole N in the $y - z$ plane emitting p_{3f} lines. The field momentum p_{3f} is along the x axis. Two positions of a Sp-2 circuit *a–b* and *b–c* in a toroid are shown rotating in the $x - y$ plane. **b** The distance of a point A on the Sp-2 circuit from the magnetic pole N is r_{2f}, taken along the *x* axis perpendicular to the pole. The Sp-2 radius is r_{2o} and the angle of rotation of point A is γ. The vector $d\hat{r}$ is tangential to the circuit at A.

Consider the face of a magnetic north pole N set in the $y - z$ plane, see Figure 6a. Let the radial field emission component p_{3f} in Fig. 4g be perpendicular to this plane along the positive *x* axis. Also, let us imagine a Sp-3 toroid with a velocity along the y axis. Figure 6a shows two positions of its Sp-2 circuit *a–b* and *b–c* which

rotate in opposite senses when viewed along the y axis. The field momentum magnitude p_{3f} is inversely proportional to the perpendicular distance r_{2f} from the plane — see Eq. (6) — so that in Cartesian coordinates [2, Eqs. (21) and (27)] with reference to Fig. 6b we have the effective magnetic momentum as

$$\vec{p}_{eff} = \vec{p}_{3f} = \frac{\hbar\alpha}{(1-\alpha^2)^{1/2} r_{2f}} \begin{pmatrix} 1 \\ 0 \\ 0 \end{pmatrix}, \qquad d\hat{r} = d\gamma \begin{pmatrix} -\sin\gamma \\ \cos\gamma \\ 0 \end{pmatrix} \tag{7}$$

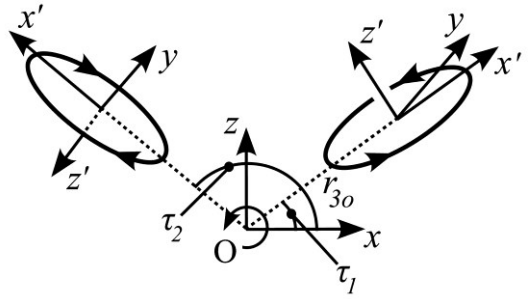

FIG. 7 Sp-3 toroid of radius r_{3o} consisting of a Sp-2 circuit rotating about the *y* axis (not to scale). The radius r_{3o} from O to the Sp-2 center is shown in two positions at angles τ_1 and τ_2 in the $x-z$ plane. Consequently, with the *y* axis having a constant orientation, the *x* and *z* axes become rotated in the $x-z$ plane to x' and z', respectively.

We now construct a Sp-3 toroid by allowing the Sp-2 circuit to rotate about the y axis through an angle τ at Sp-3 radius r_{3o}, see Fig. 7 [2, Fig. 9a]. Let us locate the center of rotation of the Sp-3 toroid O a perpendicular distance d from the magnetic north pole N. Then, since we are only interested in the distance of a point A from the magnetic pole N along the *x* axis (Fig. 6b) we have

$$r_{2f} = d + (r_{3o} + r_{2o}\cos\gamma)\cos\tau \tag{8}$$

Using Eq. (7) we also have

$$d\hat{r} = d\gamma \begin{pmatrix} -\sin\gamma\cos\tau \\ \cos\gamma \\ -\sin\gamma\sin\tau \end{pmatrix}, \quad \begin{pmatrix} x \\ y \\ z \end{pmatrix} = \begin{pmatrix} \cos\tau & 0 & -\sin\tau \\ 0 & 1 & 0 \\ \sin\tau & 0 & \cos\tau \end{pmatrix} \begin{pmatrix} x' \\ y' \\ z' \end{pmatrix} \tag{9}$$

where the first equation has made use of the given rotation matrix about the y axis. The next stage is to introduce the velocity *v* of the Sp-3 toroid that is directed along the normal to the toroidal plane and lies in the $x-y$ plane. In Fig. 8, a Sp-3 toroid is shown rotated about the *z* axis so that the direction of the velocity *v* also rotates. If the angle that the x' axis makes with the *x* axis is σ then the velocity vector runs along the y' axis and makes an angle $(\sigma + \pi/2)$ to the x axis.

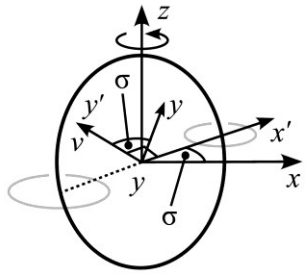

FIG. 8 Sp-3 toroid initially in the $x-z$ plane rotated an angle σ about the *z* axis to finish in the $x'-z$ plane. The velocity *v* is along y'.

The introduction of Sp-3 velocity v in relation to the momentum components that run along the x axis has the effect of producing an additional relative-to-electron momentum change in the $x-y$ plane with components

parallel to the x axis and y axis. For example, if an electron has a y component of $v\cos\sigma$ perpendicular to and approaching the field line then the field change is towards the electron with an opposite sign, see Fig. 9. The same argument applies to the x component. These changes in momentum will serve as the basis for the Lorentz force calculation. We take the speed of the source Sp-3 field component parallel to a field line to be $c' = \alpha c r_{2o}/d$, see Ref. [2, Eqs.(26) and (28)] with $d = r_{2f}$.

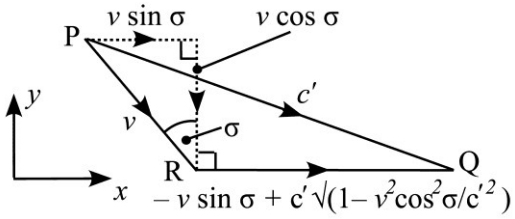

FIG. 9 The motion of the magnetic momentum field line PQ perpendicular to the magnetic pole in the Sp-3 frame due to speed v through the field at an angle σ to the y axis. This creates a change in field momentum relative to the Sp-3 center in the $x-y$ plane, where c' is the speed of the p_{3f} field component along the field line, see Eq. (10).

Figure 9 shows the magnetic momentum field passing along PQ in the Sp-3 frame as a result of the Sp-3 speed along RP. Relative to the Sp-3 frame, the field line advances along PR at speed v at an angle σ to the y axis. This has the effect of changing the field speed along the x axis in the Sp-3 frame to RQ. The field-line speed of advance along the x and y axes in that frame become $v\sin\sigma$ and $-v\cos\sigma$, respectively. We carry over the field speed ratios to the change-in-momentum ratios so, for example, $c': v\sin\sigma = 1: v\sin\sigma/c' = p_{3f}: \Delta p_x$, see the first part of Eq. (10). Then applying a rotation about the z axis using the first part of Eq. (9), we now have the magnetic momentum field change relative to the Sp-3 construction as

$$\Delta\vec{p}_{3f} = \frac{\hbar\alpha}{(1-\alpha^2)^{1/2} r_{2f}} \begin{pmatrix} \dfrac{v\sin\sigma}{c'} \\ -\dfrac{v\cos\sigma}{c'} \\ 0 \end{pmatrix}, \quad d\hat{r} = d\gamma \begin{pmatrix} -\cos\sigma\cos\tau\sin\gamma - \sin\sigma\cos\gamma \\ -\sin\sigma\cos\tau\sin\gamma + \cos\sigma\cos\gamma \\ -\sin\gamma\sin\tau \end{pmatrix},$$
$$\begin{pmatrix} x \\ y \\ z \end{pmatrix} = \begin{pmatrix} \cos\sigma & -\sin\sigma & 0 \\ \sin\sigma & \cos\sigma & 0 \\ 0 & 0 & 1 \end{pmatrix} \begin{pmatrix} x' \\ y' \\ z' \end{pmatrix} \tag{10}$$

where the middle part of Eq. (10) has made use of the last part which is the rotation matrix about the z axis.

We now consider the coordinates of point A in Fig. 6b under rotation transformations. First, we initialize the Sp-2 circuit at $\tau = 0$ in Eq. (8) and Fig. 7, then apply a y rotation of the circuit followed by a z rotation relative to the Sp-3 center O as follows:

$$\begin{pmatrix} x \\ y \\ z \end{pmatrix} = \begin{pmatrix} \cos\sigma\cos\tau & -\sin\sigma & -\cos\sigma\sin\tau \\ \sin\sigma\cos\tau & \cos\sigma & -\sin\sigma\sin\tau \\ \sin\tau & 0 & \cos\tau \end{pmatrix} \begin{pmatrix} r_{3o} + r_{2o}\cos\gamma \\ r_{2o}\sin\gamma \\ 0 \end{pmatrix} \tag{11}$$

Since we are only interested in the perpendicular distance of point A from the magnetic pole along the x axis, then after recalling that the distance to the Sp-3 center O is d, Eq. (11) leads to

$$(r_{2f})^{-1} = \frac{1}{d}\left(1 + \frac{(r_{3o} + r_{2o}\cos\gamma)\cos\sigma\cos\tau}{d} - \frac{r_{2o}\sin\sigma\sin\gamma}{d}\right)^{-1} \tag{12}$$

The calculation for the mean change in momentum around a single Sp-2 circuit taken over all Sp-3 angles τ is

$$\Delta p = \frac{N}{2\pi}\int_0^{2\pi} \vec{p}_{3f} \cdot \mathrm{d}\hat{r} \tag{13}$$

where N is the number of discrete field hits on the Sp-3 circuit in the rest time period $T_3 = h(1-\alpha^2)^{1/2}/(m_o\alpha^2c^2)$ for small speeds $\beta \ll 1$ [2, Eq. (13)]. Using Eq. (10) and a second order binomial approximation to Eq. (12) we arrive at

$$\Delta p = \frac{N\hbar r_{2o}\alpha|v|\sin\sigma'\cos\tau}{2c'd^2(1-\alpha^2)^{1/2}}\left(1-\frac{2r_{3o}\sin\sigma'\cos\tau}{d}+\cdots\right) \tag{14}$$

where $\sigma' = \sigma + \pi/2$ is the angle that the velocity vector makes with the x axis in the $x-y$ plane, see Fig. 9. This momentum change around a Sp-2 circuit arises from the change in field momentum perpendicular to the original field direction along the x axis, and is generated by the relative speed of the Sp-3 circuit and the field line. It is worth remarking that without a magnetic field gradient across a Sp-2 circuit $\Delta p = 0$.

5 Conservation of the speed of light

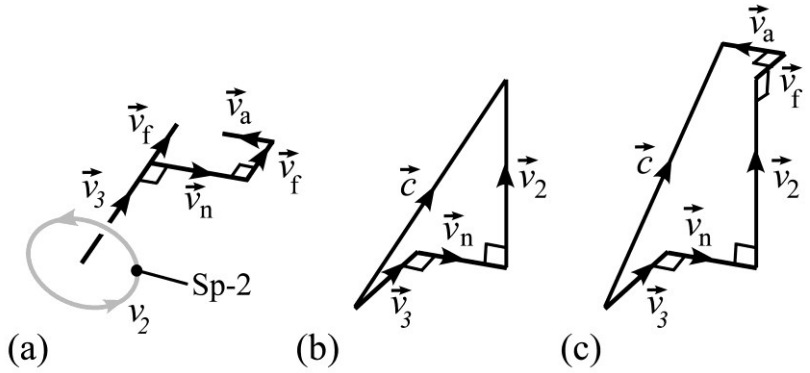

FIG. 10 a Sp-2 circuit inside a Sp-3 structure with velocity $\vec{v}_3$ along the Sp-2 normal. Vector $\vec{v}_\mathrm{n}$ is the Sp-3 normal velocity, $\vec{v}_\mathrm{f}$ is the Sp-2 circuit's response to the field altering its action, and $\vec{v}_\mathrm{a}$ is the adjustment velocity that preserves the speed of light. All four vectors are coplanar. **b** Vector diagram in a field free space that maintains the speed of light $|\vec{c}|$. The $\vec{v}_2$ is the mean Sp-2 speed resulting from the introduction of $\vec{v}_\mathrm{n}$. **c** Vector diagram for motion in a magnetic momentum field. To part **b** is now added the field effect $\vec{v}_\mathrm{f}$ on the Sp-2 circuit normal, and the light-speed restoring adjustment $\vec{v}_\mathrm{a}$.

The vector diagram in Fig. 10a shows a Sp-2 circuit whose normal is rotating at speed v_3 around the Sp-3 center (not shown). When the Sp-3 structure is stationary in a field-free space then the rotation occurs at speed $v_3 = \alpha c$, and $v_\mathrm{f} = v_\mathrm{n} = v_\mathrm{a} = 0$, where α is the fine structure constant. The Sp-2 speed of revolution is $v_2 = c(1-\alpha^2)^{1/2}$. The Sp-2 normal remains perpendicular to the Sp-3 normal even when the toroid is in motion, see Ref. [2, Section 5, Part (3)]. This means that there is no need to account for the rake angle of the Sp-3 rotational trajectory: the axis of the Sp-2 rotation is always perpendicular to the Sp-3 normal velocity vector $\vec{v}_n$. Figure 10b shows how these vectors add in a field-free space to maintain the speed of light magnitude $|\vec{c}|$. When $|\vec{v}_n| > 0$ there must be a decrease in the mean Sp-2 speed of rotation $v_2 < c(1-\alpha^2)^{1/2}$. In Figure 10c, the toroid now passes through magnetic field lines, and due to a redistribution of Sp-2 action (when the change-in-field interacts with the Sp-2 circuit), an additional speed $v_\mathrm{f,}$ is created parallel (or anti-parallel) to the Sp-2 normal along v_3. An adjustment velocity v_a is subsequently required to restore the speed of light magnitude. This whole process takes place in the Sp-2 rotation period T_2.

Let us first consider motion through a field-free space. If we set the toroid in motion with initial speed along the $v_\mathrm{n} = v$ along the toroidal axis, then while the initial v_3 component remains constant, in order to keep the speed of light constant, the mean Sp-2 rotational speed v_2 must be given by

$$v_2 = c\left(1-\frac{v_3^2+v_\mathrm{n}^2}{c^2}\right)^{1/2} \tag{15}$$

where $v_3 = \alpha c$. This is the v_2 component that is perpendicular to both $\vec{v}_3$ and $\vec{v}_\mathrm{n}$, see Fig. 10b.[16] As we shall see, the index k will enable an iterative calculation to be performed once field effects are introduced.

We now pass the toroid through magnetic field lines set across its path. The mean Sp-2 rotational action is either overloaded or underloaded, and the gain or loss of momentum is redistributed along the direction of $\vec{v}_3$ as $\vec{v}_\mathrm{f}$, being a velocity resulting from the field interaction. This occurs in Sp-2 time period T_2. The calculation uses Eq. (14), where for relativistic electron mass m we have

$$v_\mathrm{f} = \frac{\Delta p}{m} = A(\sigma', \tau)\frac{|v_\mathrm{n}|}{m}, \quad A(\sigma', \tau) = \frac{N\hbar r_{2o}\alpha \sin\sigma' \cos\tau}{2c'd^2(1-\alpha^2)^{1/2}}\left(1 - \frac{2r_{3o}\sin\sigma'\cos\tau}{d} + \cdots\right) \tag{16}$$

Equation (15) now needs adjusting so that

$$c^2 = \left(v_3 + v_f\right)^2 + (v_n + v_a)^2 + v_2^2 \tag{17}$$

Combining Eqs. (15) and (17) we obtain a quadratic in v_a that only requires the input of the translational speed v_n and the Sp-3 rotational speed v_3:

$$v_\mathrm{a} = -v_\mathrm{n}\left(1 - \sqrt{1 - \frac{v_f^2}{v_n^2} - 2\frac{v_3 v_f}{v_n^2}}\right) \sim -A\frac{v_3}{v_n} - \frac{A^2}{2}\left(1 + \frac{v_3^2}{v_n^2}\right) \tag{18}$$

We then adjust the speed of the Sp-3 circuit along its original direction through the field as follows:

$$v_\mathrm{n} \to v_\mathrm{n} + v_\mathrm{a} \sim v_\mathrm{n}\left(1 - \frac{Av_3}{v_n} - \frac{A^2}{2}\left(1 + \frac{v_3^2}{v_n^2}\right)\right) \tag{19}$$

Since $v_\mathrm{n} = v$ as the speed the toroid enters the field and the Sp-3 speed as v_3, we can ensure that the speed of light in the toroidal circuit remains a constant.

Average taken over all Sp-2 locations

We now calculate the mean momentum change along the x axis and z axis, see Fig. 7. Each location of the Sp-2 circuit center as it travels around the Sp-3 circuit is characterized by a value of τ.

(a) Equation (14) shows that when $-\pi/2 < \tau < \pi/2$ we have $\Delta p > 0$ $(0 < \sigma' < \pi)$ and the Sp-2 circuit increases in momentum along its normal. This is to be redistributed into v_f (see Fig. 10) which is tangential to the Sp-3 rotation.

(b) For $\pi/2 < \tau < 3\pi/2$ we find $\Delta p < 0$ so that the Sp-2 circuit loses momentum. This amounts to a gain in momentum in the opposite direction.

Let us consider Eq. (14) with the adjustment in Eq. (19). The Sp-3 normal lies along y', see Fig. 8. Projecting the vector v_f (which lies along the z' axis in Fig. 7) onto the x axis with v_n in Eq. (14) replaced by v_n from Eq. (19), we find

$$\Delta p_x = -\frac{1}{\pi}\int_{-\frac{\pi}{2}}^{\frac{\pi}{2}} \Delta p \sin\tau \, \mathrm{d}\tau = 0 \tag{20}$$

[16] The components parallel and antiparallel to $\vec{v}_\mathrm{n}$ are proportional to $v_2 = c(1-\alpha^2)^{1/2} \pm v_\mathrm{n}$, and they cancel out when summing the incremental magnitudes around the Sp-2 circuit. In contrast, the components perpendicular to $\vec{v}_\mathrm{n}$ have no $\pm v_\mathrm{n}$ but a reduction factor $(1 - (v_\mathrm{n}/c')^2)^{1/2}$. With a decrease in mean Sp-2 speed we should expect the mean Sp-2 radius to increase to preserve angular momentum.

From the discussion in (a) and (b), the direction of momentum change in the z direction is the same for a point at $-z$ as it is for one at $+z$, see Fig. 7. Noting the identity for c', the mean Δp_z is given by

$$\Delta p_z = \frac{1}{\pi}\int_{-\frac{\pi}{2}}^{\frac{\pi}{2}} \Delta p \cos\tau \ \mathrm{d}\tau \sim \frac{N\hbar|v_\mathrm{n}|\sin\sigma'}{4cd(1-\alpha^2)^{1/2}}\left(1-\frac{16r_{3o}\sin\sigma'}{3\pi d}+\cdots\right) \tag{21}$$

For a relatively weak field strength — determined by N, the number of discrete field hits in time T_2 — where $A(\sigma',\tau) \ll 1$ our approximations will hold. Eq. (21) applies to a Sp-2 clockwise rotation when looking along the z' axis, combined with a Sp-3 counter clockwise rotation when viewed along the y axis, see Fig. 7. This case is shown in Fig. 11a. The momentum in the positive z direction in Eq. (21) mirrors the behaviour of a negative charge moving through a magnetic field.

6 The nature of charge

For $\beta \ll 1$, we find the change in momentum in Eq. (21) using the Sp-3 time period $T_3 = h(1-\alpha^2)^{1/2}/(m_o\alpha^2c^2)$ of a Sp-3 circuit at rest [2, Eq. (13)]. Dividing Eq. (21) by T_3 gives a force

$$F_z = \frac{\Delta p_z}{T_3} = Q_2Q_3\frac{Nm_o\alpha^2c|v_\mathrm{n}|\sin\sigma'}{8\pi(1-\alpha^2)d} \tag{22}$$

while keeping in view that N is the field-absorption count in time T_3. Here, $Q_2 = +1$ when the Sp-2 rotation is clockwise viewed in the positive z direction at $\tau = 0$, and $Q_2 = -1$ when counter clockwise; and $Q_3 = +1$ when the Sp-3 rotation is counter-clockwise viewed in the positive y direction, and $Q_3 = -1$ when clockwise, see Figs. 7 and 11. Changing the direction of the Sp-3 rotation means that an action overload in the Sp-2 circuit increases the speed of its normal in the opposite direction. When $Q_2Q_3 = +1$, the Sp-3 is deflected in the positive z direction thereby acting as a negative charge would. Conversely, for $Q_2Q_3 = -1$ it moves in the negative z direction and acts like a positive charge. This means there are two chiralities that can be associated with a negative charge and two for a positive one, see Fig. 11.

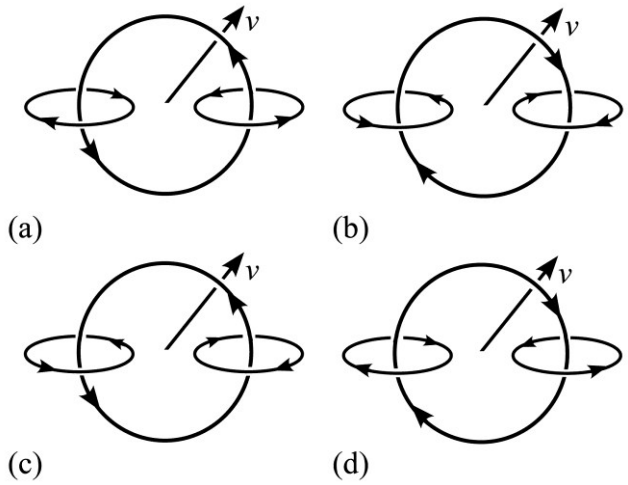

FIG. 11 The four cases of charge chirality viewed in the Sp-3 direction of motion. **a** Negative charge $Q_2 = +1,\ Q_3 = +1$. **b** Negative charge $Q_2 = -1,\ Q_3 = -1$. **c** Positive charge $Q_2 = -1,\ Q_3 = +1$. **d** Positive charge $Q_2 = +1,\ Q_3 = -1$.

It is now only a small step to generalize to the Lorentz force so that a comparison with Eq. (1) suggests that

$$q|\vec{B}| = Q_2 Q_3 \frac{N m_o \alpha^2 c}{8\pi(1-\alpha^2)d} \tag{24}$$

A calibration of N with $|\vec{B}|$ for various d should then be possible from experiment. It should also be noted that if the speed v in Fig. 11a is reversed, as might occur if a reference frame carrying the magnetic pole accelerates past it, we arrive at the arrangement in Fig. 11b which is classed here as the same charge.[17] However, since $\sigma' \to \sigma' + \pi$ in Eq. (22), the direction of deflection is also reversed.

7 Electric fields

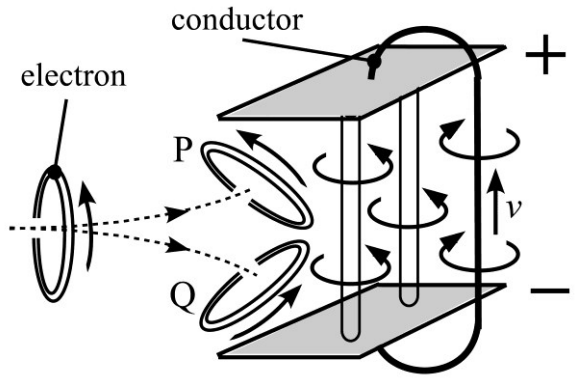

FIG. 12 Ionized electron approaching two parallel plates. The conductor connecting the two plates has a counter clockwise momentum field in the direction of the electron velocity v. The continuity of field rotation means that the electric field tubes between the plates rotate clockwise moving from negative to positive. If the electron P approaches the upper plate, the electron and field rotations oppose and there is attraction. At Q, the rotations are same sense and constitute a repulsion.

We now suppose that when a potential difference is applied across a conducting wire, the motion of the electrons as Fig. 11a along the conductor from the negative to the positive plate causes their toroidal axes to align, see Figure 12. Consequently, their electric field momenta rotate around the wire counter clockwise when viewed in their direction of motion. The electric field tubes between the plates continue this rotation, being counter clockwise from the positive to the negative plate. This means that when the ionized electron approaches the positive plate at P their rotations oppose and cause an attraction as in the hydrogen atom. If instead it approaches the negative plate at Q their rotations reinforce to produce a repulsion.

8 Conclusions

We have shown how it is possible to obtain the Lorentz force law of deflection from a mass represented as a Sp-2 (optical OAM). The motion of the Sp-3 configuration towards a field line set across its path generates a field momentum perpendicular to the field line. This interacts with the various orientations of the Sp-2 (optical OAM) circuit in the Sp-3 rotation of the moving mass. If the field strength had no variation along the x axis (see Fig. 6a), there would be no net change-in-momentum field (generated by the toroidal motion along the y axis) when integrated around a Sp-2 circuit. However, since the magnetic momentum varies with d, the perpendicular distance from the pole, the field strength on the magnetic pole side of the Sp-2 is different from that on the opposite side. This excess or deficit of momentum integrated around the Sp-2 circuit is then redistributed along the Sp-2 normal.

The theory presented here, based on the principles of the photonic toroidal vortex (PTV) model set out in Ref. [2], suggests a geometrical nature of charge in terms of a combination of Sp-2 and Sp-3 rotations. As far as the PTV theory of the hydrogen atom is concerned [2], it reinforces the assumption that an ‘electron’ Sp-2 orbiting in a Sp-3 toroid has two Sp-2 rotation senses, see Figs. 11a and 11c. This duality has been shown to be crucial for the hydrogen hyperfine interaction [21] and lends credit to the claim of consistency in the PTV theory. It also

[17] When reversing the speed direction of the Sp-3, the view of Fig. 11a from the right side becomes the view of Fig. 11b from the left side.

raises the possibility that when the proton–electron Sp-2 rotation senses are in opposition in a hydrogen atom [21], the electron becomes a *positron* — Fig 11a becomes Fig 11c, both at electron scale. However, it is never ionized as a positron but only as an electron that reverts back to its lowest action Sp-2 sense (Fig. 11a) on release with the same sense as the proton (Fig. 11c). So the "stealth positron" is never observed due to structural suppression at ionization by the least action principle that favours the electron. This might account for the infrequent observation of free positrons in comparison with free electrons.

References

1. Faraday, M., On lines of magnetization of light and the illumination of magnetic lines of force, Experimental Researches in Electricity, Nineteeth series (November 1845).
2. Clarke, B. R., A photonic toroidal vortex model of the hydrogen atom fine structure, Quantum Studies: Mathematics and Foundations **12**, 19 (2025), https://doi.org/10.1007/s40509-025-00364-9.
3. Beth, R. A., Mechanical detection and measurement of the angular momentum and light, Physical Review **50** (1936): 115–25.
4. Moothoo,D. N., J. Arlt, R. Conroy, F. Akerboom, A. Voit, and K. Dholkia, Beth's experiment using optical tweezers, American Journal of Physics **69** (2001): 271–276.
5. Allen, P. J., A radiation torque experiment, American Journal of Physics **34** (1966): 1185–1192.
6. Garetz, B. A., and S. Arnold, Variable frequency shifting of circularly polarized laser radiation via a rotating half-wave retardation plate, Optical Communications **31** (1979): 1–3.
7. Bretenaker, F., and A. Le Floch, Energy exchanges between a rotating retardation plate and a laser beam, Physical Review Letters **65** (1990): 2316–7.
8. Beijersbergen, M. W., R. P. C. Coerwinkel, M. Kristensen, and J. P. Woerdman, Helical wavefront laser beams produced with a spiral phaseplate, Optics Communications **112** (1994): 321–27.
9. Soskin, M. S., V. N. Gorshkov, M. V. Vasnetsov, J. T. Malos, and N. R. Heckenberg, Topological charge and angular momentum of light beams carrying optical vortices, Physical Review A **56** (1997): 4064–4075, Fig. 5.
10. Tang, D. Y., N. R. Heckenberg, and C. O. Weiss, Phase dependent helical pattern formation in a laser, Optics Communications **114** (1995): 95–100.
11. He, H., M. E. J. Friese, N. R. Heckenberg, and H. Rubinsztein-Dunlop, Direct observation of transfer of angular momentum to absorptive particles from a laser beam with a phase singularity, Physical Review Letters **75** (1995): 826–29.
12. Courtial, J., and M. J. Padgett, Performance of a cylindrical mode converter for producing Laguerre–Gaussian modes, Optics Communications **159** (1999): 13–18.
13. Padgett, M., J. Arlt, N. Simpson, and L. Allen, An experiment to observe the intensity and phase structure of Laguerre–Gaussian laser modes, American Journal of Physics **64** (1996): 77–82.
14. Allen, L., M. W. Beijersbergen, R. J. C. Spreeuw, and J. P. Woerdman, Orbital angular momentum of light and the transformation of Laguerre–Gaussian laser modes, Physical Review A **45** (1992): 8185–8189.
15. Simpson, N. B., K. Dholakia, L. Allen, and M. J. Padgett, Mechanical equivalence of spin and orbital angular momentum of light: an optical spanner, Optics Letters **22** (January 1997): 52–54.
16. Friese, M. E., J. Enger, H. Rubinsztein-Dunlop, and N. R. Heckenberg, Optical angular momentum transfer to trapped absorbing particles, Physical Review A **54** (1996): 1593–1596.
17. Wan, C., Q. Cao, J. Chen, A. Chong, and Q. Zhan, Toroidal vortices of light, Nature Photonics **16** (2022): 519–522; Supplementary information https://doi.org/10.1038/s41566-022-01013-y, Fig. S5a.
18. Uchida, M., and A. Tonomura, Generation of electron beams carrying orbital angular momentum, Nature **464** (2010): 737–739. (doi:10.1038/nature08904)
19. Veerbeck, J., H. Tian, and P. Schattschneider, Production and application of electron vortex beams, Nature **467** (2010): 301–304. (doi: 10.1038/nature09366)
20. McMorran, B. J., A. Agrawal, I. M. Anderson, A. A. Herzing, H. J. Lezec, J. J. McClelland, and J. Unguris, Electron vortex beams with high quanta of orbital angular momentum, Science **331** (2011): 192–95. (doi:10.1126/science.1198804)
21. Clarke, B. R., A hydrogen atom hyperfine structure from a photonic toroidal vortex model, Atoms (MDPI) under peer review (2026).
22. Maxwell, J. C., On physical lines of force Part II, The London and Edinburgh Philosophical Magazine and Journal of Science, fourth series (March 1861): 338–348.
23. Maxwell, J. C., A dynamical theory of the electromagnetic field, Philosophical Transactions of the Royal Society of London **155** (1865): 459–512.

24. Maxwell, J. C., On physical lines of force Part III, The London and Edinburgh Philosophical Magazine and Journal of Science, fourth series (April and May 1861): 12–24.
25. Maxwell, J. C., A Treatise on Electricity and Magnetism (1873). Dover Publications, 1954.
26. Yaghjian, A. D., Maxwell's derivation of the Lorentz force from Faraday's law, Progress in Electromagnetic Research M **93** (2020): 35–42.
27. Heaviside, O., On the electromagnetic effects due to the motion of electrification through a dielectric, Philosophical Magazine, (April 1889): 324–339.
28. Heaviside, O., The general solution of Maxwell's electromagnetic equations in a homogeneous isotropic medium, The London, Edinburgh, and Dublin Philosophical Magazine, Series 5 **27** (Jan. 1889): 29– 50.
29. Clarke B. R., Reinterpretation of the Grangier experiment using a multiple-triggering single-photon model, Modern Physics letters B **37**, 15 (2023) https://doi.org/10.1142/S0217984923500422
30. Faraday, M., On lines of magnetic force; their definite character; and their distribution within a magnet and through space, Experimental Researches in Electricity, Twenty-eighth series (December 1852): 25–56.

On behalf of all authors, the corresponding author states that there is no conflict of interest.